Stress Changes the Material State of a Bacterial Biomolecular Condensate and Shifts its Function from mRNA Decay to Storage

Luis A. Ortiz-Rodríguez[1], Hadi Yassine[2,3], Ali Hatami[4], Vidhyadhar Nandana[2], Christopher A. Azaldegui[5], Jiayu Cheng[1], Yingxi Zhu[4], Jared M. Schrader[2,3*], Julie S. Biteen[1,5*]

[1]Department of Chemistry, University of Michigan, Ann Arbor, MI 48109 USA.

[2]Departments of Chemistry and Biological Sciences, Wayne State University, Detroit, MI 48202 USA.

[3]Department of Biology, Indiana University, Bloomington, IN 47405 USA.

[4]Department of Chemical Engineering and Materials Science, Wayne State University, Detroit, MI 48202 USA.

[5]Doctoral Program in Chemical Biology, University of Michigan, Ann Arbor, MI 48109, USA.

[*]To whom correspondence should be addressed: jsbiteen@umich.edu, jaschrad@iu.edu

Abstract

Bacterial ribonucleoprotein bodies (BR-bodies) are dynamic biomolecular condensates that play a pivotal role in RNA metabolism. We investigated how BR-bodies significantly influence mRNA fate by transitioning between liquid- and solid-like states in response to stress. With a combination of single-molecule and bulk fluorescence microscopy, biochemical assays, and quantitative analyses, we determine that BR-bodies promote efficient mRNA decay in a liquid-like condensate during exponential growth. On the other hand, BR-bodies are repurposed from sites of mRNA decay to reservoirs for mRNA storage under stress; a functional change that is enabled by their transition to a more rigid state, marked by reduced internal dynamics, increased molecular density, and prolonged residence time of ribonuclease E. Furthermore, we manipulated ATP levels and translation rates, and we conclude that the accumulation of ribosome-depleted mRNA is a key factor driving BR-body rigification, and that condensate maturation further contributes to this process. Upon nutrient replenishment, stationary-phase BR-bodies disassemble, releasing stored mRNAs for rapid translation, demonstrating that BR-body function is governed by a reversible mechanism for resource management. These findings reveal adaptive strategies by which bacteria regulate RNA metabolism through condensate-mediated control of mRNA decay and storage.

Introduction

Biomolecular condensates are dynamic macromolecular assemblies that often form via phase separation,[1,2] a reversible process that enables the cell to respond rapidly to environmental changes.[3] These assemblies are selectively permeable and can exchange client molecules.[1,4] Depending on their physical state, which can range from liquid droplets to hydrogels and insoluble aggregates, condensates facilitate various biological functions.[1,5] Liquid-like condensates promote biochemical reactions by allowing internal

35 diffusion and exchange with the dilute phase, while gel- and solid-like condensates have reduced diffusion
36 and exchange, which slow down biochemical reactions and may potentially sequester biomolecules for
37 storage.[1,2] Notably, transitions from the liquid to solid state in biomolecular condensates have been linked
38 to neurodegenerative protein aggregation disorders:[6,7] reducing the fluidity of these condensates can
39 negatively affect their function.[8,9] However, in other cases, such as germ granules, solid-like states play
40 important roles in mRNA storage and translational control in the developing embryo.[10]

41 Recently, biomolecular condensates have emerged as a broadly utilized mechanism for organizing
42 diverse biochemical pathways within the bacterial cytoplasm,[11–19] and this organizational paradigm is
43 particularly important in bacteria because these organisms generally lack membrane-bound organelles.[20,21]
44 Bacterial ribonucleoprotein bodies (BR-bodies), the organelles that contain the RNA degradation machinery,
45 were the first bacterial condensates demonstrated to assemble via liquid-liquid phase separation (LLPS),
46 driven by interactions between the large intrinsically disordered region (IDR) of ribonuclease E (RNE; Fig. 1a)
47 and RNA.[11]

48 *Caulobacter crescentus* BR-bodies share functional similarities with eukaryotic processing bodies
49 (P-bodies) and stress granules (SGs), as all three contain the mRNA decay machinery. RNE (Fig. 1a), the
50 core scaffold and driver of BR-body function, is the essential and rate-limiting factor in bacterial mRNA
51 decay.[22,23] Similarly, Xrn1 is a core component of eukaryotic P-bodies and SGs, and it controls cytoplasmic
52 mRNA decay.[24–26] In addition, similar types of molecules are enriched in BR-bodies (Fig. 1b,c), P-bodies, and
53 SGs, including DEAD-box RNA helicases, Lsm proteins, miRNAs, small-RNAs, and translationally repressed
54 mRNAs.[27] P-bodies and SGs have been predominantly studied under conditions of cell stress, and some
55 studies indicate that P-bodies promote mRNA decay, while others show an mRNA storage function,
56 whereas SGs have only been found to promote storage.[11,25,28] These differences in the decay and storage
57 functions are correlated with differences in the mobility of molecules within P-bodies[25,28–31] and SGs,[32–34]
58 since P-bodies have been found to have higher mobility and more rapid exchange with the dilute phase than

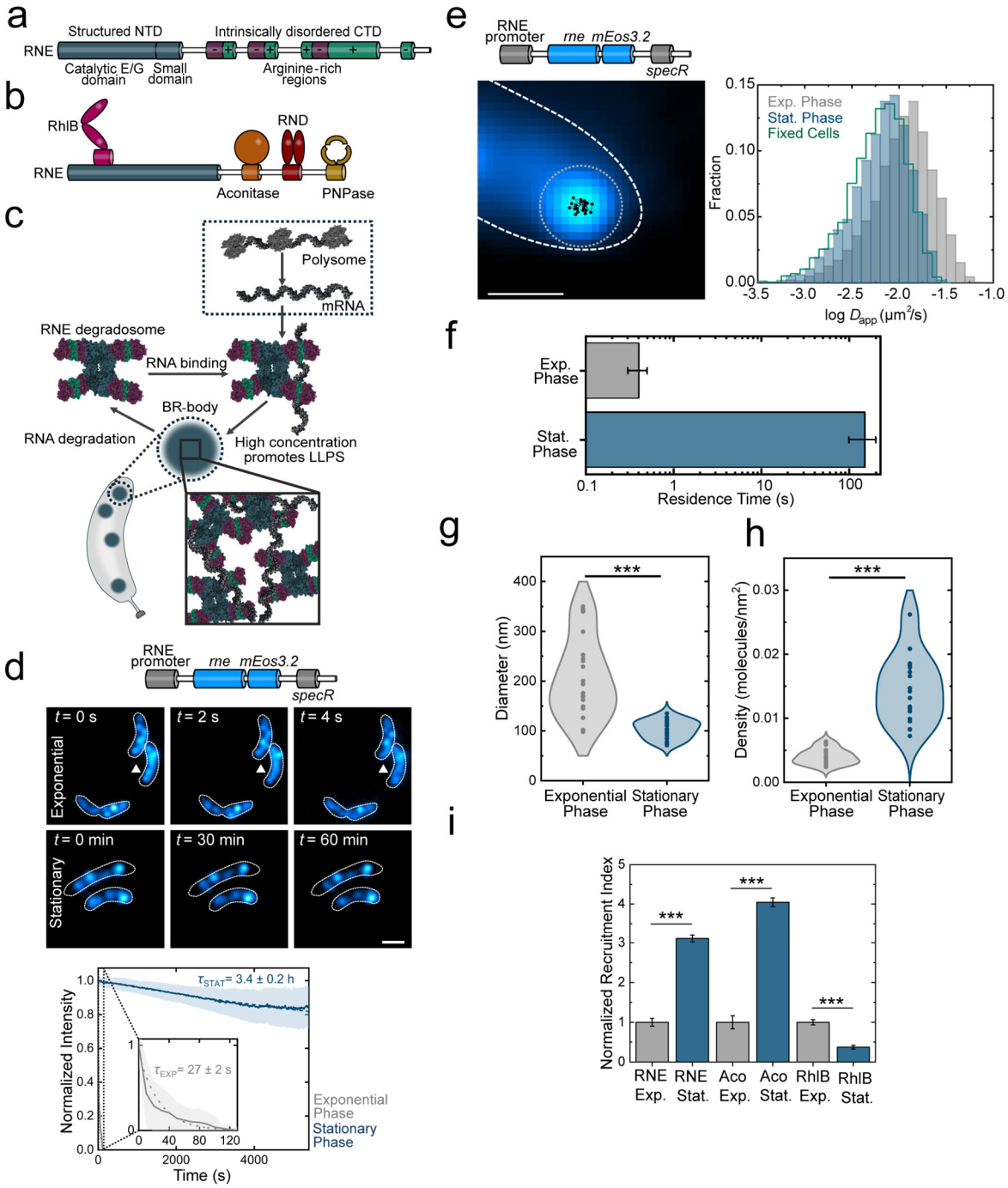

Fig. 1 | BR-bodies are dynamically arrested and compacted upon entering stationary phase.

Fig. 1 | BR-bodies are dynamically arrested and compacted upon entering stationary phase. (a) Domain organization of *C. crescentus* RNase E (RNE). (b) The *C. crescentus* RNA degradosome includes RNE, RhlB, aconitase, RNase D, and PNPase. The RNE NTD has an RhlB binding site. The CTD has interaction sites for aconitase, RNase D, and PNPase. (c) In the working model for BR-body-mediated mRNA decay, untranslated mRNAs and the RNE degradosome can phase separate into a biomolecular condensate, thereby increasing their local concentration and accelerating decay processes within the BR-body. The condensate dissolves as mRNA is degraded, releasing degradosome components and oligonucleotides. (d) Lifespans of condensates based on an RNE-mEos3.2 construct (top). Middle: representative images of *C. crescentus* cells (white outlines) and RNE-mEos3.2 (blue) in each phase as a function of imaging time, *t*; arrowheads indicate representative RNE-mEos3.2 foci. Scale bar: 500 nm. Bottom: decay profiles of photobleaching-corrected intensities with estimates of the average condensate lifespans, τ_{EXP} and τ_{STAT}, in exponential and stationary phases, respectively. Analyses include N = 427 foci in 881 cells (exponential) and N = 932 foci in 3,543 cells (stationary). (e-i) Dynamics of degradosome components within BR-bodies across growth phases. (e) Single-molecule tracking of RNE inside BR-bodies. Top-left: genetic construct used to track RNE. Bottom-left: a representative single-molecule trajectory of RNE-mEos3.2 within a BR-body (dotted circle) in a *C. cresentus* cell (dashed lines). The black dots indicate the super-localized positions of the molecule in consecutive 20-ms imaging frames. Scale bar: 500 nm. Right: Changes in the diffusivity of RNE within BR-bodies across growth phases. The apparent diffusion coefficients for RNE-mEos3.2 trajectories in live cells are compared to apparent diffusion coefficients of trajectories in fixed cells to distinguish between diffusing and static molecules. (f) Increase in residence time of RNE-mEos3.2 of BR-bodies between exponential and stationary phase. (g) Increase in BR-body diameter between exponential and stationary phases. The BR-body diameter is estimated as the maximum span of the cluster identified using density-based cluster analysis. (h) Increase in the density of RNE-mEos3.2 single-molecule localizations within BR-bodies during the transition from exponential to stationary phase. Each point shows the density in one condensate. (i) Normalized recruitment index, NRI, of degradosome components RhlB-PAmChy, Aco-PAmChy, and RNE-mEos3.2 inside the BR-bodies in stationary phase relative to the recruitment in exponential phase, indicating the presence of incomplete degradosomes in BR-bodies during stationary phase. Error bars represent propagated standard deviations. The NRI values were each normalized by the mean of the corresponding exponential phase NRI. The error for each condition was calculated from the original standard deviation using standard error propagation rules. Error bars in f and i: standard deviation from three biological replicates. *** in g and i denotes $p < 0.001$.

59 SGs. BR-bodies have been predominantly studied in exponentially growing bacteria cells, during which they
60 appear to have liquid-like properties that promote mRNA decay (Fig. 1c).[11,35] In contrast, under cell stress,
61 BR-bodies undergo increased condensation that correlates with enhanced survival under these conditions,
62 yet their internal dynamics and rates of mRNA degradation have not been previously explored under stress.[11]
63 Evidence from multiple bacterial species has shown that mRNA decay rates are reduced under conditions
64 of nutrient limitation, such as when cells enter stationary phase, yet the role of BR-bodies in this slowdown
65 of mRNA decay has not yet been explored.[36–41]

66 In this study, we investigate changes in the dynamics within BR-bodies between exponential growth
67 and stationary phase and how these differences impact the mRNA decay pathway. We define the material
68 state of a biomolecular condensate as the set of physical properties that determine internal mobility,
69 exchange with the surrounding environment, condensate compaction, and thus biological function.
70 Furthermore, in this work, a condensate is considered liquid-like when it exhibits dynamic internal
71 rearrangement, rapid molecular exchange with the surrounding environment, lower biomolecular density,
72 and short residence times of key components, while rigid condensates show reduced internal molecular
73 diffusion, longer component residence times, increased compaction, and reduced exchange with the
74 surrounding environment. Our live-cell single-molecule microscopy results demonstrate that BR-bodies
75 transition from a dynamic, liquid-like state during exponential growth to a less dynamic, more rigid material
76 state during stress. We demonstrate that this transition is associated with a functional shift from enhancing
77 mRNA decay in exponential phase to promoting mRNA storage in the rigid state. In line with these results,
78 we measure that the *in vitro* maturation of RNE condensates and subsequent arrest of dynamics lead to a
79 strong reduction in RNE activity. Given the similarities between BR-bodies and eukaryotic biomolecular
80 condensates like SGs and P-bodies, our findings further suggest that differences in cell growth conditions
81 may also alter the material properties of P-bodies and SGs to shift the inherent preferences for mRNA decay
82 vs. storage across diverse organisms.

83 **The transition from exponential to stationary phase is associated with BR-body rigidification**

84 To investigate the dynamics of molecules within BR-bodies and their response to stress, we labeled
85 the endogenous copy of RNE with the green-to-red photoconvertible fluorescent protein mEos3.2 (RNE-
86 mEos3.2; Fig. 1d).[42] This labeling strategy allows us to study the properties of BR-bodies as a whole using
87 bulk fluorescence in the initial mEos3.2 green state, and to measure their internal dynamics at the single-
88 molecule level in the mEos3.2 red state after photoconversion using 405-nm excitation. We compared BR-
89 body dynamics during exponential and stationary growth phases to understand the effect of non-invasively
90 induced cellular starvation, ensuring physiologically relevant observations of the stress response. We
91 further sought to resolve two previous confounding observations: (1) there is an increased number of BR-
92 bodies and a higher copy number of RNE in each condensate in cells at stationary phase,[11] a nutrient-
93 deprived state during which bacterial growth and division cease, and yet (2) mRNA decay is slower in
94 stationary phase.

95 To investigate how stationary phase alters BR-bodies, we performed time-lapse imaging of cells in
96 exponential and stationary phases. In exponential phase, BR-bodies rapidly assemble and disassemble,
97 consistent with their known role in mRNA decay (Fig. 1d, Supplementary Movie 1). However, in stationary
98 phase, BR-bodies are dramatically stabilized (450-fold; Fig. 1d, Supplementary Movie 2). As RNA is required
99 for BR-body phase separation,[11] the decreased dissolution rate of BR-bodies during stationary phase
100 suggests reduced RNA decay activity, as mRNA degradation is necessary for BR-body disassembly (Fig.
101 1c).[11] Single-molecule tracking of RNE-mEos3.2 and the degradosome protein aconitase-PAmChy,
102 previously identified as a direct binding partner to RNE[11,43,44] and a core component of the *C. crescentus* RNA
103 degradosome, revealed significantly reduced diffusivity of RNE and its degradosome client proteins within
104 BR-bodies during stationary phase (Fig. 1e and Extended Data Fig. 1), consistent with a more rigid internal
105 microenvironment. In addition, we compared RNE-mEos3.2 diffusion in both growth phases with the
106 apparent diffusion of immobile RNE-mEos3.2 molecules in fixed cells. While we measure slow diffusion of

107 RNE-mEos3.2 within BR-bodies during exponential phase, this value is higher than our lower bound as
108 determined in fixed cells. In contrast, the diffusion profile of RNE-mEos3.2 in stationary phase cells closely
109 matches that of fixed cells, suggesting that, under our experimental conditions, RNE-mEos3.2 is essentially
110 static within the BR-bodies during stationary phase. Furthermore, the residence time of RNE within BR-
111 bodies is 370-fold longer in stationary phase compared to exponential phase (Fig. 1f). After identifying the
112 RNE-mEos3.2 clusters with a density-based cluster analysis,[45] we determined the molecular density and
113 estimated the BR-body diameter, $\bar{d}$, as the maximum span of each cluster (Fig. 1g,h). In exponential phase,
114 the BR-bodies are less dense and larger ($\bar{d}$ = 206 ± 2 nm) than in stationary phase ($\bar{d}$ = 102 ± 1 nm) (mean ±
115 SEM; $p < 0.001$). Importantly, the decreased diffusivity and increased residence time of RNE within the BR-
116 bodies, along with their compaction, are also observed under ethanol stress, indicating that dynamic arrest
117 behavior likely occurs under other inducing stresses (Extended Data Figs. 1,2). This compaction explains
118 the decreased internal dynamics, where the rigid state constrains RNE within the BR-body.

119 We also analyzed the diffusion of RNE outside the BR-bodies in both exponential and stationary
120 phase cells to determine whether the observed changes in RNE mobility were specific to the condensate
121 internal microenvironment. The mobility of RNE molecules not associated with the BR-bodies remained
122 unchanged between growth phases (Extended Data Fig. 1), indicating that the reduced mobility observed
123 within BR-bodies during stationary phases arises from changes in the condensate internal
124 microenvironment rather than reflecting overall cellular changes between growth phases.

125 To determine whether BR-bodies retain characteristics of phase-separated condensates during
126 stationary phase, rather than forming irreversible aggregates, we treated cells with 5% 1,6-hexanediol (HD),
127 a commonly used aliphatic alcohol that disrupts the weak hydrophobic interactions essential for phase
128 separation.[46–48] BR-bodies dissolve within ~ 25 minutes of HD treatment (Extended Data Fig. 1), confirming
129 that they remain sensitive to HD despite rigidification during stationary phase. This finding suggests that BR-

130 bodies retain hallmark features of biomolecular condensates, even in the rigid state, and that the observed
131 rigidification reflects a dynamic arrest rather than a transition to an aggregated or misfolded state.

132 BR-bodies concentrate the RNA degradosome complex, which in *C. crescentus* contains aconitase,
133 RhlB, and PNPase (Fig. 1b).[11,44] We quantified the recruitment of aconitase and RhlB to BR-bodies during
134 exponential and stationary phases, normalizing by differences in overall expression levels. After
135 normalization, we found that aconitase recruitment increases 4-fold, while RhlB recruitment decreases 3-
136 fold in stationary phase (Fig. 1i). These results reveal a stoichiometric reorganization of BR-bodies under
137 stress. In particular, the concomitant loss of RhlB and enrichment of RNE and aconitase indicate the
138 presence of incomplete degradosomes inside BR-bodies during stationary phase. DEAD-box RNA helicases
139 are central regulators of biomolecular condensates;[49] their ATPase cycle maintains the condensates in a
140 dynamic, non-equilibrium state, facilitating the enrichment of client molecules and buffering the dispersed
141 ribonucleoprotein pool. The decreased recruitment of the DEAD-box RNA helicase RhlB thus likely impairs
142 the internal remodeling of BR-bodies, potentially contributing to their rigidification during stress.

143 **Increased levels of poorly translated mRNA and maturation trigger the transition to the rigid**
144 **material state**

145 During stationary phase, bacterial cells encounter nutrient scarcity, which slows down
146 cellular processes including metabolic activity, leading to lower ATP levels (Fig. 2a).[50] Reduced ATP
147 levels subsequently impact various processes, including protein synthesis and translation, promote
148 phase separation of proteins with intrinsically disordered regions (IDRs),[18] contribute to protein
149 aggregation,[12,13] and cause physical changes in cytoplasm,[51,52] creating a glassy state that slows the
150 diffusion of mesoscale objects such as BR-bodies. Additionally, since DEAD-box helicases like RhlB
151 require ATP hydrolysis to remodel, dissolve, cooperatively bind RNA,[53] prevent strong interactions,

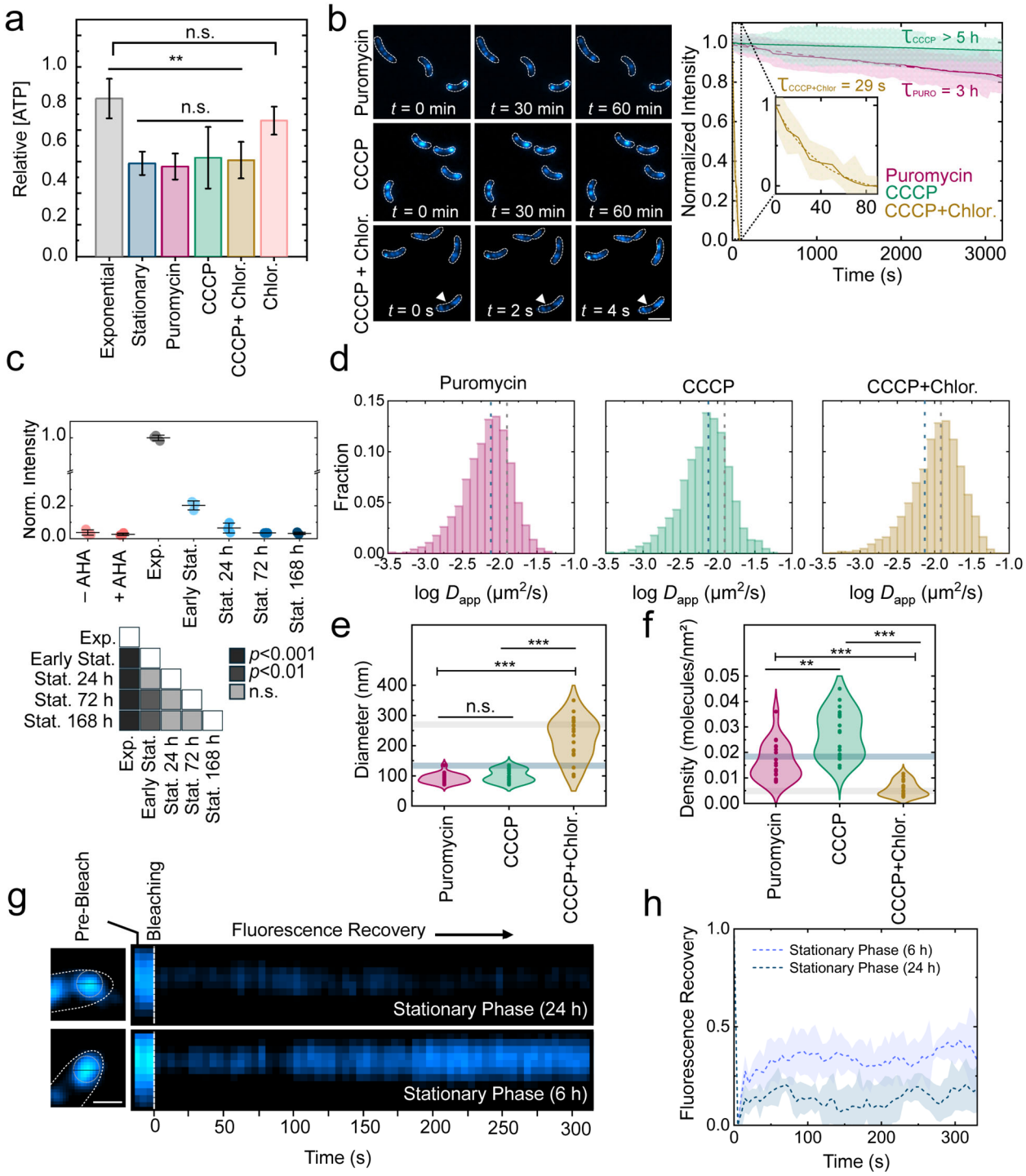

Fig. 2 | Rigidification of BR-bodies is promoted by increased levels of poorly translated mRNAs.

Fig. 2 | Rigidification of BR-bodies is promoted by increased levels of poorly translated mRNAs. (a) Quantification of intracellular ATP concentrations in *C. crescentus* using a luciferase-based assay following no treatment or treatment as described. ATP levels are normalized to exponential growth levels. (b) Lifespans of BR-bodies in cells under the acute treatment conditions described in (a). Left: Representative images of RNE-mEos3.2 (blue) in *C. crescentus* cells (white outlines) as a function of treatment and imaging time, *t*. Arrowheads indicate representative RNE-mEos3.2 foci. Scale bar: 2 μm. Right: Decay profiles of photobleaching-corrected intensities used to estimate the average condensate lifespan. Analyses include $N = 308$, 347, and 241 foci for puromycin, CCCP, and CCCP + chloramphenicol, respectively. (c) Top: relative translational levels in exponential and stationary phases using Biorthogonal Non-Canonical Amino Acid Tagging (BONCAT), and controls with azidohomoalanine (AHA) and chloramphenicol and without AHA. Error bars: standard deviation of three replicates. Bottom: statistical analysis. (d) Impact of acute treatments on the diffusivity of the BR-body RNE scaffold. The distribution of apparent diffusion coefficients for RNE-mEos3.2 trajectories is measured following each treatment. Vertical dashed lines: distribution medians. (e) Effect of acute treatments on the BR-body diameter, which is estimated as the maximum span of the cluster identified using density-based cluster analysis following each treatment. Horizontal lines indicate the mean of the distribution of exponential phase and stationary phase BR-body diameters. (f) Changes in the density of RNE-mEos3.2 single-molecule localizations within BR-bodies following each treatment. Horizontal lines indicate the mean of the distribution of exponential phase and stationary phase BR-body densities. (g) Dynamics inside BR-bodies in cells during prolonged stationary phase. Representative fluorescence recovery after photobleaching (FRAP) experiment kymographs during early (6 h) and late (24 h) stationary phase cells showing the bleaching and recovery of the RNE-mEos3.2 foci (blue) as a function of time, *t*. Scale bar: 500 nm. (h) FRAP of RNE-mEos3.2 in cells at the early and late stationary phase. $N = 20$ foci. Error bars in a and c: standard deviation from three biological replicates. Statistics in a, e, and f: *** denotes $p < 0.001$, ** denotes $p < 0.005$, and n.s. denotes $p > 0.05$.

152 and maintain the fluidity of the condensates,[49] the low ATP levels at stationary phase may impair
153 these activities.

154 To separate the effects of low ATP levels and reduced translation on BR-body rigidification,
155 we artificially decreased ATP and translation levels in exponential phase cultures of *C. crescentus*.
156 To lower ATP levels, we treated the cultures with the protonophore carbonyl cyanide *m*-chlorophenyl
157 hydrazone (CCCP) to disrupt the proton motive force,[54] rapidly inhibiting ATP synthase. A 20-min
158 treatment with 100 μM CCCP was found to reduce cellular ATP concentrations to levels comparable
159 to those observed during stationary phase (Fig. 2a). To reduce translation levels, we used puromycin
160 (150 μg/mL for 30 min), which prematurely cleaves peptide chains[55] and releases ribosome subunits
161 and mRNA, thereby increasing the availability of ribosome-depleted transcripts in the cytoplasm.
162 Since puromycin treatment also results in ATP levels similar to those observed in stationary phase
163 (Fig. 2a), we treated cells with CCCP and the translation elongation inhibitor chloramphenicol as a
164 control. Chloramphenicol prevents translation by blocking peptide bond formation and
165 accumulating ribosomes on mRNA.[56] Interestingly, treating exponential phase cultures with CCCP
166 and puromycin leads to long-lived BR-bodies (Fig. 2b), similar to those observed during stationary
167 phase (Fig. 1d). However, when cells are treated with the combination of CCCP and
168 chloramphenicol, BR-bodies remain short-lived, similar to those observed during exponential phase
169 in the absence of stress (Fig. 2b). Similarly, BR-bodies remain short-lived when cells are treated with
170 chloramphenicol only (Supplementary Figure 1). This finding suggests that the increased lifespan of
171 BR-bodies upon treatment with CCCP might be an indirect effect of dropping ATP levels inhibiting
172 translation rather than directly related to ATP availability. Translation is typically the most energy-
173 intensive process during exponential growth,[57,58] and ATP and GTP are essential for several steps in
174 translation, including the esterification of amino acids to tRNAs, selection of the aa-tRNAs to the
175 ribosome, the assembly of ribosomal subunits, and the translocation of ribosomes along the mRNA.

176 When NTP levels are decreased, these processes slow, resulting in reduced translation rates.
177 Additionally, biorthogonal non-canonical amino acid tagging (BONCAT) revealed a significant
178 decrease in translation levels during the late stationary phase, with reductions of 30-fold, as well as
179 in cells treated with puromycin, CCCP, and the combination of CCCP and chloramphenicol, all
180 relative to exponential phase (Fig. 2c, Extended Data Fig. 3).

181 Similar to the extended lifespan of BR-bodies observed upon treatment with CCCP and
182 puromycin, these treatments also replicated stationary-phase decreases in RNE-mEos3.2 diffusivity
183 inside the BR-bodies (Fig. 2d), BR-body size (Fig. 2e), RNE molecular density (Fig. 2f), and residence
184 time within BR-bodies (Extended Data Fig. 2). Conversely, cells treated with a combination of CCCP
185 and chloramphenicol do not rigidify. This finding suggests that the rigid material state transition in
186 stationary phase state requires increased amounts of ribosome-free mRNA transcripts in the
187 cytoplasm, whereas ATP scarcity alone is insufficient.

188 We identified low ribosome occupancy as a key factor contributing to the rigid material state
189 of BR-bodies during stationary phase. However, under prolonged stress, biomolecular condensates
190 have been observed to mature from having liquid-like to solid-like properties.[1,59–63] Initially, their
191 components interact transiently: molecules freely rearrange and exchange with the surrounding
192 phase, resembling liquid behavior. Over time, mechanisms such as entanglement of disordered
193 polypeptides,[64] vitrification,[65] percolation,[66] and nucleation and elongation of amyloid-like fibers[67]
194 contribute to rigidification and decreased molecular dynamics.[68] We investigated the role of
195 maturation in BR-body rigidification by *in vivo* fluorescence recovery after photobleaching (FRAP) of
196 BR-bodies (RNE-mEos3.2) in cultures of *C. crescentus* cells at 6 hrs and 24 hrs into stationary phase
197 (Fig. 2g,h). The condensates become less dynamic over time in stationary phase. The BR-body
198 fluorescence recovers only minimally at both time points, consistent with a rigid material state, but
199 BR-bodies are slightly more dynamic at 6 hrs than at 24 hrs. To further investigate the role of

200 maturation, we reconstituted the system *in vitro* and extracted meaningful information based on
201 RNE, the first bacterial protein found to undergo LLPS at physiological concentrations without
202 crowding agents.[11] FRAP performed on RNE droplets reconstituted *in vitro* and aged with RNA for 30
203 min, 4 hrs, and 8 hrs (Extended Data Fig. 4) revealed that condensates aged for 30 min were
204 significantly more dynamic, with nearly full fluorescence recovery within 2.5 min, whereas
205 condensates aged for 4 hrs exhibited minimal recovery and 8 hrs were even less dynamic. These
206 results support the role of maturation in changing the material state of BR-bodies.

207 **The material state transition of BR-bodies during stress shifts their function from promoting**
208 **mRNA decay to facilitating mRNA storage**

209 Our *in vivo* and *in vitro* results establish that, during stress conditions, the internal dynamics
210 and structure of BR-bodies become more rigid. Previous two-color images of mRNA and RNE using
211 MS2 RNA labeling[69] and fluorescence *in situ* hybridization (FISH) during exponential growth have
212 shown that transcripts such as *rsaA* exhibit low colocalization (~28%) with RNE in BR-bodies in
213 conditions allowing active RNA degradation.[35] However, colocalization increases significantly (~80%)
214 when RNE endonuclease cleavage is blocked using an RNE active site mutation (ASM) involving the
215 two residues coordinating the catalytic Mg^{2+} ion in the active site[35], which, taken together, suggest
216 mRNA decay within BR-bodies during exponential growth. These results suggest that the transition
217 to a more rigid material state, along with its associated effects, may enable BR-bodies to store mRNA
218 during stress conditions.

219 To investigate the role of BR-bodies in mRNA storage, we performed two-color imaging of RNE
220 and mRNA using a live-cell MS2 system and FISH, and we measured mRNA degradation rates using
221 quantitative reverse transcription polymerase chain reaction (qRT-PCR). Notably, this study employs
222 an MS2 system optimized to accurately track short-lived mRNAs.[70] We selected four key mRNA

223 transcripts needed for *C. crescentus* exponential growth: *rsaA*, *rne*, *spmX*, and *ctrA*. All four mRNAs
224 were previously found to be stabilized in an RNE-IDR truncation mutant incapable of making BR-
225 bodies, suggesting that BR-bodies play a role in their degradation.[35,71] The RsaA S-layer protein is the
226 most abundant protein in *C. crescentus*.[72] RsaA was chosen for comparison with the prior result,
227 where RNE cleavage was blocked using the ASM, providing insight into the role of the catalytic activity
228 of RNE in the condensate and its effect on transcript recruitment into BR-bodies.[35] RNE is crucial in
229 RNA processing, degradation,[22,23] BR-body formation, and cell fitness.[11] The integral membrane
230 protein SpmX enables cell division by localizing the histidine kinase DivJ to the stalked pole.[73,74]
231 Finally, CtrA is a master regulator of the cell cycle; it controls chromosome replication and
232 transcription, and it modulates the expression of about 25% of cell cycle-regulated genes in *C.*
233 *crescentus*.[75–79] These strategically selected transcripts enabled us to thoroughly assess the role of
234 BR-bodies in mRNA storage under stress and to determine the relevance of the stored transcripts.

235 Images of MS2-labeled *ctrA*, *spmX*, and *rsaA* transcripts (Fig. 3a,b, and Extended Data Fig. 5)
236 highlight their higher recruitment to BR-bodies during stationary phase compared to exponential
237 phase; these data sets were quantified using Pearson correlation coefficients (PCC). All transcripts
238 colocalize more with BR-bodies during stationary phase, similar to the behavior of *rsaA* when RNE
239 cleavage is blocked, suggesting significantly lower degradation activity by RNE during this phase. This
240 mRNA RNE colocalization is further confirmed by FISH (Supplementary Figure 2). To ensure that the
241 observed differences in BR-body colocalization across growth phases reflect transcript-specific
242 recruitment dynamics rather than analytical artifacts or changes in overall transcript abundance, we
243 used transfer-messenger mRNA (tmRNA) as a negative control. tmRNA is abundant in *C. crescentus,*
244 and is strongly depleted from the BR-bodies with a $\log_2$ fold-change of −2.8.[35] Applying the same
245 colocalization analysis to the target transcripts, we found that tmRNA colocalizes significantly less
246 with BR-bodies (PCC = 0.13 ± 0.04) compared to all other transcripts, even during exponential phase

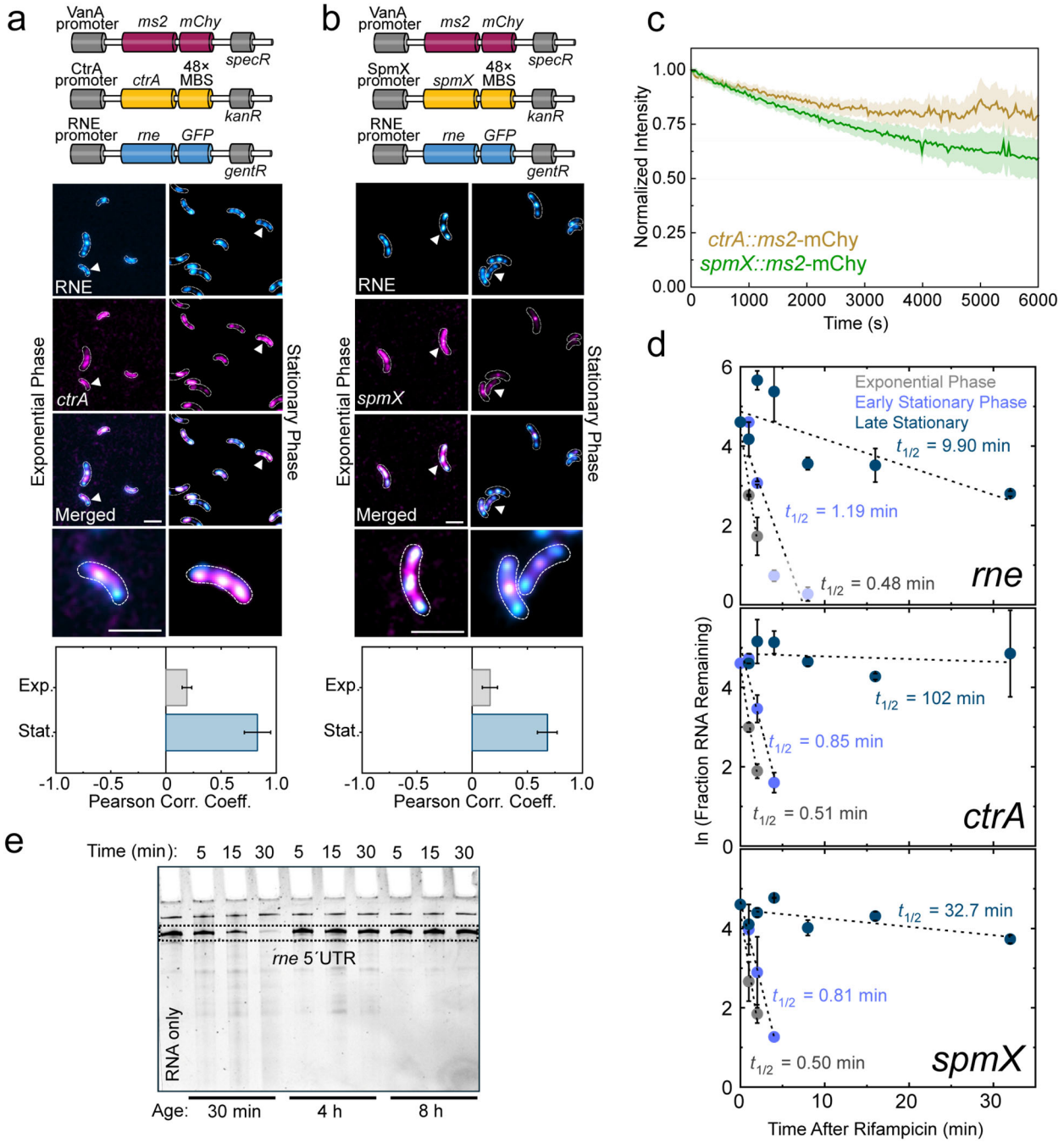

Fig. 3 | Rigidification of BR-bodies switches their function from mRNA decay to storage of key growth mRNAs.

Fig. 3 | Rigidification of BR-bodies switches their function from mRNA decay to storage of key growth mRNAs. (a,b) Stability of the *ctrA* (a) and *spmX* (b) transcripts in BR-bodies. Top: genetic constructs used to observe the transcript stability within the BR-bodies *in vivo*. Middle: Representative two-color images showing higher recruitment of the *ctrA* and *spmX* transcripts (magenta) to BR-bodies (blue) during stationary phase (left) relative to exponential phase (right). The merged channel is shown on two magnification levels for clarity. Bottom: Differences in recruitment quantified by the Pearson correlation coefficients between channels. Error bars: standard deviation from 20 foci analyzed per phase. *** denotes $p < 0.001$. Arrowheads indicate representative foci. Scale bars in (a) and (b): 2 μm. (c) Decay profiles of *ctrA* and *spmX* in the late stationary growth phase. Analyses include $N = 108$ and 174 foci for the *ctrA* and *spmX* transcripts, respectively. (d) qRT-PCR measurements of RNA half-lives for *rne*, *ctrA*, and *spmX* transcripts highlight the changes in transcript stability from exponential phase to the late stationary phase. Error bars: standard deviation from three biological replicates. (e) Condensate aging leads to decreased RNE cutting activity *in vitro*, as evidenced by the *rne* mRNA band in a 7% urea TBE/PAGE gel.

247 (Supplementary Figure 3). These results confirm that the high levels of colocalization observed for
248 specific transcripts during stationary phase are not simply due to increased transcript abundance;
249 rather, they reflect selective recruitment into BR-bodies under stress.

250 We also assessed the stability of these transcripts tagged with MS2-RNA hairpins by
251 analyzing the photobleaching-corrected intensities of MS2-mChy foci colocalized with RNE foci
252 during both growth phases (Fig. 3c and Extended Data Fig. 5). To ensure that our observations
253 accurately reflect transcript stabilization and not artifacts of the labeling system, we employed two
254 versions of the MS2 system which are both utilized with a MS2-mChy dimerization deficient variant:[80]
255 a 48×-array with weaker MS2 coat protein RNA hairpin affinity[70] and a 96×-array.[35] Previous studies
256 have demonstrated that binding of the coat protein to MS2 binding sites artifactually stabilizes
257 mRNA.[81–83] Therefore, we confirmed that any observed accumulation of the mChy signal within BR-
258 bodies was due to real transcript stabilization and not an effect of the labeling system. As shown in
259 Fig. 3a,b, mChy foci do not colocalize with BR-bodies during exponential phase when using the 48×-
260 array system. However, using the 96×-array version (Extended Data Fig. 5), we observed mChy foci
261 colocalizing with BR-bodies, even during exponential phase. Despite the potential transcript
262 stabilization caused by the more perturbing 96×-array MS2 system, we still observed significant
263 differences in the decay profiles between exponential and stationary phases. During exponential
264 phase, MS2-mChy (96×-array) foci disassemble in under a few min, consistent with rapid internal
265 decay of mRNAs (Extended Data Fig. 5). In contrast, during stationary phase, MS2-mChy (48×-array)
266 foci and stably colocalize with BR-bodies for significantly longer, indicating slowed mRNA decay (Fig.
267 3c and Extended Data Fig. 5). To investigate the observations of the MS2-tagged RNAs, we measured
268 the RNA decay rates. mRNA half-life measurements by qRT-PCR confirmed this stabilization: *rne*,
269 *spmX*, and *ctrA* exhibit 20-, 65-, and 200-fold stability increases, respectively, from exponential to
270 late stationary phase (Fig. 3d), and were confirmed by mRNA FISH for *ctrA* mRNA and *spmX* mRNA

271 (Supplementrary Figure 4). To test whether stabilization in stationary phase depends on BR-body
272 formation, we measured the stability of *spmX* and *ctrA* transcripts in stationary phase cultures of *C.*
273 *crescentus* expressing RNE-ΔCTD; these cells cannot assemble BR-bodies.[11] In this background,
274 transcript stabilization was reduced to only ~3-fold, confirming that BR-bodies are essential for the
275 pronounced stabilization of mRNA during stress (Supplementary Figure 4). Together, these
276 measurements suggest that the rigid state of RNE is associated with a dramatic slowdown in mRNA
277 decay activity, consistent with a model in which BR-body material state regulates RNA turnover.

278 The RNA chaperone Hfq is a well-known regulator of RNA stability, and, in *E. coli*, Hfq has
279 been observed to form condensates with RNA under conditions of nutrient deprivation, where it has
280 also been observed to colocalize with *E. coli* RNE.[16,84,85] In *C. crescentus*, Hfq has been observed to
281 colocalize to a subpopulation of BR-bodies,[43] suggesting that it might impact the stability of
282 transcripts in the rigid BR-bodies observed in stationary phase. To test whether Hfq contributes to
283 transcript stabilization, we measured *ctrA* mRNA decay in a *Δhfq* background. In exponentially
284 growing *Δhfq* cells, *ctrA* mRNA decays slightly more slowly than in wild-type cells, but still degrades
285 rapidly (Supplementary Table 1), indicating that Hfq is not required for rapid turnover in exponential
286 phase. In stationary phase, *ctrA* mRNA remains highly stable in *Δhfq* cells, similarly to wild type,
287 suggesting that Hfq is not required for BR-body-mediated transcript stabilization. Consistently, the
288 diffusion profile of RNE-mEos3.2 within BR-bodies remains unchanged in the *Δhfq* background
289 (Supplementary Figure 6), indicating that the change to the rigid material state does not depend on
290 Hfq. Hence, the stabilization during stationary phase is independent of Hfq and instead reflects
291 protection conferred by the BR-body environment itself. As an additional control, we measured the
292 stability of tmRNA, a highly abundant transcript that is not enriched in the BR-bodies. tmRNA
293 remained fully stable in both exponential and stationary phases (> 8 min and > 16 min half-lives,
294 respectively), confirming that transcripts not recruited into BR-bodies do not exhibit phase-

295 dependent changes in decay rate. This finding further supports the model that BR-body-mediated
296 stabilization depends on selective mRNA recruitment.

297 To investigate whether the reduced RNA cleavage activity of RNE is a direct result of
298 rigidification, we assessed the cutting activity of RNE in 30-min, 4-hr, and 8-hr *in vitro*-reconstituted
299 condensates (Fig. 3e). These aged RNE droplets were formed with RNE and RNA, but without Mg^{2+},
300 an essential cofactor for RNA cleavage by RNE. At each droplet age, RNA cleavage was initiated by
301 adding Mg^{2+}, and samples were collected at various time points to assay RNA cleavage.[71] RNE
302 efficiently cleaves the *rne* 5' UTR in droplets aged for only 30 min,[71] with the corresponding band in
303 the PAGE gel disappearing within 30 min of Mg^{2+} addition (Fig. 3e). In contrast, virtually no RNA
304 cleavage was observed in the rigidified droplets at the 4-hr and 8-hr timepoints. This finding suggests
305 that maturation into the rigid state can directly shut off RNE cleavage. Furthermore, we hypothesize
306 that BR-body formation during stress serves as a repository for mRNA and a means to sequester RNE
307 and potentially other degradative enzymes in an inactive state. This hypothesis is supported by the
308 higher amount of RNE in condensates during stationary phase, and by our recent work, where we
309 demonstrated that overexpression of RNA during exponential phase leads to growth arrest. Taken
310 together with our *in vitro* results, these results support a model in which BR-body rigidification
311 reduces RNE activity, allowing for selective preservation of mRNAs during stress.

312 **Fluidized BR-bodies are capable of the functional release of mRNAs**

313 Stored mRNAs may be useful for growth-arrested cells either by acting as a nutrient source
314 to promote regrowth or by being released to ribosomes to restart the translation program upon the
315 addition of new nutrients. To determine if mRNA release and subsequent translation can occur after
316 cells exit stationary phase and enter exponential growth, we assessed whether rigidification is
317 reversible by observing if stationary-state BR-bodies fluidize over time after nutrient replenishment

318 (Extended Data Fig. 6). Indeed, BR-body disassembly was detected after 90 min of nutrient
319 replenishment. We further investigated transcript storage by BR-bodies post-nutrient replenishment
320 by monitoring the colocalization of the *spmX* transcript with BR-bodies in stationary phase cultures
321 (Supplementary Figure 5). After 3 hrs, the colocalization profile of *spmX* with BR-bodies returns to
322 that observed during exponential phase (i.e., PCC = 0.22 ± 0.05 vs. 0.25 ± 0.04 in Fig. 3b), suggesting
323 that stored mRNA exits BR-bodies upon removal of stress.

324 Additionally, to evaluate whether these transcripts could be translated after exiting BR-
325 bodies, we designed a series of experiments to distinguish between translation from pre-existing
326 transcripts and newly transcribed mRNAs. In wild-type *C. crescentus*, nutrient replenishment after
327 stationary phase led to substantial RNE-mEos3.2 fluorescence recovery over 6 hours following
328 whole-cell bleaching (Fig. 4a,b). To determine whether this recovery reflects translation of stored
329 transcript, we first inhibited new RNA synthesis using rifampicin. Under these conditions, RNE
330 fluorescence still recovered, indicating that recovery does not require transcription of new mRNAs
331 and must arise from mRNAs that existed prior to rifampicin treatment. To confirm that this recovery
332 reflects active translation rather than delayed protein maturation, we inhibited translation with
333 chloramphenicol, which abolished fluorescence recovery, indicating that the signal arises from
334 newly synthesized protein and not from maturation of pre-existing fluorescent proteins.

335 We then asked whether BR-bodies are required for this post-stress recovery. In cells
336 expressing RNE-ΔCTD, which are unable to form BR-bodies, fluorescence recovery for SpmX-
337 mEos3.2 and RNE-ΔCTD-mEos3.2 was minimal following nutrient replenishment, similar to the
338 translation-inhibited wild-type cells (Fig. 4a,b). This result indicates that BR-bodies are required to
339 maintain mRNAs in a translatable state during stationary phase. Importantly, we observed a similar
340 behavior for *spmX* and *rne* transcripts, suggesting that BR-body-mediated transcript storage and
341 translation upon release is a general mechanism not limited to *rne*. To confirm the presence of full-

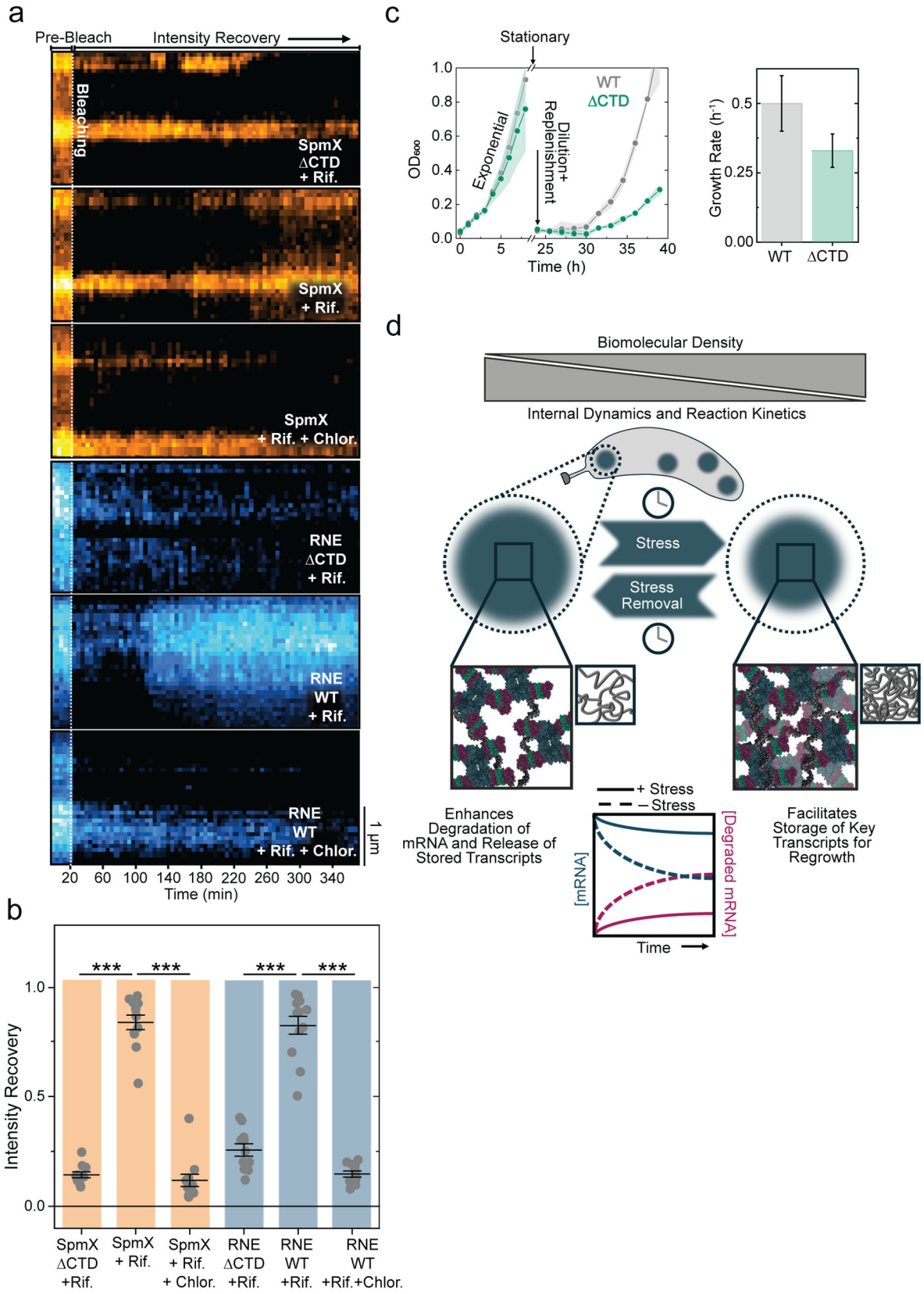

Fig. 4 | Stored mRNAs can be translated and promote rapid growth.

Fig. 4 | Stored mRNAs can be translated and promote rapid growth. (a) Representative kymographs of SpmX-mEos3.2 in both wild-type RNE and ΔCTD-RNE backgrounds, and of wild-type RNE and RNE-ΔCTD-mEos3.2 alone. Kymographs were generated by measuring cell fluorescence intensity along the long axis of stationary-phase *C. crescentus* cells after nutrient replenishment and inhibition of new transcript synthesis and translation with rifampicin and chloramphenicol, respectively. (b) Quantification of the recovery of the integrated intensity over the whole cell area at t = 6 h relative to t = 0 h following photobleaching of the whole cell intensity. Each dot below the distribution corresponds to the recovered intensity in one cell (n = 12 cells), and the error bars indicate the standard error. *** denotes $p < 0.001$. (c) Functional implications of mRNA storage in BR-bodies. Left: comparison of the growth rate of *C. crescentus* cells with wild-type RNE vs. cells with RNE-ΔCTD (incapable of forming BR-bodies) when cultures are back-diluted into PYE medium after 24 h in stationary phase. Right: growth rates following nutrient replenishment; error bars indicate the standard error. Cells expressing RNE-ΔCTD grow more slowly following nutrient replenishment. (d) Proposed model for how the material state of BR-bodies tunes their activity, enabling a transition from mRNA decay enhancement during growth to storage during stress.

342 length mRNA that is capable of being translated within stationary phase BR-bodies, we amplified the
343 full-length *ctrA* mRNA by RT-PCR and found that full-length mRNA is indeed present within the BR-
344 body (Extended Data Fig. 5c). The observed translation of released mRNA from BR-bodies suggests
345 that BR-bodies can store functionally intact mRNAs for later translation upon stress removal.

346 We ultimately assessed the functional implications of stress-induced mRNA storage in BR-
347 bodies by comparing the growth rate of *C. crescentus* cells with wild-type RNE to cells with RNE-
348 ΔCTD after 24 hrs in stationary phase (Fig. 4c). Remarkably, cells with RNE-ΔCTD exhibit a 1.5-fold
349 reduction in growth rate and a lag phase that is 3 hrs longer compared to the wild-type strain following
350 nutrient replenishment. To distinguish the role of BR-body formation from potential pleiotropic
351 effects of disrupting degradosome assembly, we analyzed recovery dynamics in an RNE-ΔDBS strain,
352 which lacks the degradosome binding sites on RNE and therefore cannot assemble the RNA
353 degradosome, but still forms condensates.[11] Upon nutrient replenishment, RNE-ΔDBS cells recover
354 with kinetics comparable to wild-type (Supplementary Figure 7), in contrast to the slow recovery
355 observed in the RNE-ΔCTD strain (Fig. 4b,c). These results indicate that degradosome assembly is
356 not required for the efficient exit from stationary phase, and instead support the conclusion that the
357 formation of BR-bodies and their ability to store essential transcripts during stress play a critical role
358 in enabling recovery. Thus, this functional separation-of-function mutant demonstrates that the loss
359 of condensate formation, rather than general defects in RNA metabolism, compromises recovery in
360 the RNE-ΔCTD mutant.

361 Altogether, these results suggest that during stress, BR-bodies play a critical role in storing
362 essential transcripts, which are then readily available for translation upon return to nutrient-repleted
363 conditions, contributing to a faster transition into exponential growth. This storage mechanism
364 circumvents the need to synthesize new transcripts, thereby facilitating the rapid program of protein
365 production necessary for regrowth. Importantly, we observed in *Agrobacterium tumefaciens* and

366 *Sinorhizobium meliloti* liquid-like BR-bodies also rigidify in stationary phase (Extended Data Fig. 7),
367 suggesting that the material state transition to mRNA storage may be a general feature of BR-bodies.

368 **Discussion**

369 BR-bodies are multifunctional biomolecular condensates that orchestrate RNA decay and
370 store RNA transcripts during stress (Fig. 4d). Under prolonged stress, BR-bodies rigidify, resulting in
371 decreased internal dynamics, higher biomolecular density, and compaction. This transition extends
372 the residence time of RNE within these condensates, reduces its degradation activity, and leads to
373 an altered degradosome deficient in RhlB. Consequently, RNA transcripts within BR-bodies are
374 stabilized under adverse conditions. Although a significant portion of RNE and mRNAs are
375 distributed outside BR-bodies, our data indicate that BR-body-localized RNE plays the dominant role
376 in transcript stabilization during stationary phase.

377 The stabilization of mRNA within BR-bodies is a functional bacterial adaptation that allows
378 the preservation of valuable epigenetic information during exposure to a variety of different stressors.
379 Upon stress removal, environmental and cellular conditions shift, triggering the restoration of
380 dynamics and disassembly of BR-bodies. This change facilitates the release of stabilized transcripts
381 back into the cytoplasm, where they can be promptly translated to support recovery and growth. This
382 elegant mechanism, wherein bacteria dynamically modulate the physical and biochemical
383 properties of BR-bodies in response to environmental cues, leverages phase separation and enzyme
384 kinetics to exert temporal and spatial control over RNA degradation and utilization. This mechanism
385 underscores how bacteria use biomolecular condensates not just as active enzymatic reaction sites
386 but also as adaptive tools for managing genetic resources to ensure survival and adaptation in
387 fluctuating environments.

388 The bacterial aggresome is another subcellular organelle that has recently been reported to
389 store mRNA under arsenic stress in *E. coli*.[12,13,86,87] Our results indicate that, like aggresomes, BR-
390 bodies store mRNA transcripts during stress conditions. However, the putative mechanisms by
391 which aggresomes and BR-bodies stabilize mRNA differ significantly from one another. Aggresomes
392 have been proposed to protect mRNA by excluding ribonucleases, with protein surface charge
393 playing a crucial role.[86] Aggresomes are thought to assemble through protein aggregation, and
394 although protein chaperones are enriched within aggresome structures, the molecular trigger of their
395 phase separation has not been uncovered.[12] However, whether aggresomes in *E. coli* might exclude
396 RNE,[88–90] the major mRNA decay nuclease, has not yet been explored. In contrast, RNE is the central
397 scaffold necessary for BR-body formation,[11] and rather than RNE being excluded from mature BR-
398 bodies, the material properties of the BR-bodies shut off the RNase activity. Interestingly, *C.*
399 *crescentus* BR-bodies have been found to enrich the aggresome marker proteins HslU, DnaK, and
400 ClpB,[43] suggesting some functional similarity to aggresomes, yet aggresomes have a dark color in
401 phase-contrast microscopy, whereas no such dark aggregates have been observed in *C. crescentus*
402 at stationary phase nor following heat shock, antibiotic treatment, or other stresses.[11,35,91,92]

403 Despite the mechanistic data in the current study, it is still unclear how mRNA stored within
404 BR-bodies is protected from RNE cleavage when cells transition from stationary to exponential
405 phase. Potential models for future research include the possibility that *C. crescentus* possesses RNE
406 inhibitor proteins stored within BR-bodies, similar to *E. coli* RraA and RraB.[93,94] Another hypothesis is
407 that the RNE catalytic domain is completely denatured during rigidification and requires refolding by
408 protein chaperones to become active again during the transition back to exponential growth.

409 Overall, we have determined that the function of the BR-bodies as sites of mRNA storage or
410 decay is dictated by their material state. This model of BR-bodies underscores their role as versatile
411 biomolecular condensates and also demonstrates how biophysical properties influence the

412 biochemical function of condensates. The ability to modulate enzymatic activity through controlled
413 biophysical changes within these condensates reveals a novel paradigm of gene expression
414 regulation, which is pivotal for bacterial survival in fluctuating environments.

415 **Data Availability**

416 All data generated and analyzed during this study are included in this published article and its
417 Supplementary Information files. Raw source data is available upon request.

418 **Code Availability**

419 Data processing and analysis scripts for this study were written in MATLAB and Python. The code
420 generated for this study is available on Github. Image analysis scripts:
421 https://github.com/BiteenMatlab/bacterial_condensates; and SMALL-LABS algorithm package:
422 https://github.com/BiteenMatlab/SMALL-LABS.

423 **Acknowledgments**

424 The authors acknowledge the support of NIH grant R35GM124733 to J.M.S., NIH T32GM142519-03
425 to H.Y., and NIH grants R01GM143182 and R01GM144731 to J.S.B. The authors thank Dr. Anthony
426 Vecchiarelli for generously providing access to his wide-field fluorescence microscope. Thanks to Dr.
427 Tamara Hendrickson and the WSU Department of Chemistry for lab space and equipment after the
428 Schrader lab was destroyed in a fire.

429 The authors declare no competing interests.

430 **Author contributions**

431 L.A.O.-R. designed, performed, and analyzed experiments (all live-cell single-molecule and
432 ensemble fluorescence imaging, FRAP, FISH, growth curves, and ATP level measurements),

433 interpreted results, and wrote the manuscript. H.Y. designed, performed, and analyzed experiments
434 (strain construction, qRT-PCR, and BONCAT) and interpreted results. V.N., A.H., and Y.Z. designed,
435 performed, and analyzed experiments (all *in vitro*-reconstitution and *in vitro* FRAP experiments) and
436 interpreted results. C.A.A. analyzed experiments (developed a script to isolate trajectories inside the
437 condensates) and contributed to writing the revised manuscript. J.C. analyzed experiments (cluster
438 analysis). J.M.S. provided expertise in the design and construction of the strains, interpreted results,
439 and wrote the manuscript. J.S.B. provided expertise in the design of live-cell imaging experiments,
440 designed experiments, interpreted results, and wrote the manuscript.

References

441 1. Banani, S. F., Lee, H. O., Hyman, A. A. & Rosen, M. K. Biomolecular condensates:
442 organizers of cellular biochemistry. *Nat. Rev. Mol. Cell Biol.* **18,** 285–298 (2017).
443 2. Boeynaems, S., Alberti, S., Fawzi, N. L., Mittag, T., Polymenidou, M., Rousseau, F.,
444 Schymkowitz, J., Shorter, J., Wolozin, B., Bosch, L. V. D., Tompa, P. & Fuxreiter, M.
445 Protein Phase Separation: A New Phase in Cell Biology. *Trends Cell Biol.* **28,** 420–435
446 (2018).
447 3. Yoo, H., Triandafillou, C. & Drummond, D. A. Cellular sensing by phase separation:
448 Using the process, not just the products. *J. Biol. Chem.* **294,** 7151–7159 (2019).
449 4. Ditlev, J. A., Case, L. B. & Rosen, M. K. Who's In and Who's Out—Compositional Control
450 of Biomolecular Condensates. *J. Mol. Biol.* **430,** 4666–4684 (2018).
451 5. Nakamura, H., DeRose, R. & Inoue, T. Harnessing biomolecular condensates in living
452 cells. *J. Biochem. (Tokyo)* **166,** 13–27 (2019).
453 6. Aguzzi, A. & Altmeyer, M. Phase Separation: Linking Cellular Compartmentalization to
454 Disease. *Trends Cell Biol.* **26,** 547–558 (2016).

455 7. Ramaswami, M., Taylor, J. P. & Parker, R. Altered Ribostasis: RNA-Protein Granules in
456 Degenerative Disorders. *Cell* **154,** 727–736 (2013).
457 8. Zhu, L., Richardson, T. M., Wacheul, L., Wei, M.-T., Feric, M., Whitney, G., Lafontaine, D.
458 L. J. & Brangwynne, C. P. Controlling the material properties and rRNA processing
459 function of the nucleolus using light. *Proc. Natl. Acad. Sci.* **116,** 17330–17335 (2019).
460 9. Dorone, Y., Boeynaems, S., Flores, E., Jin, B., Hateley, S., Bossi, F., Lazarus, E.,
461 Pennington, J. G., Michiels, E., Decker, M. D., Vints, K., Baatsen, P., Bassel, G. W.,
462 Otegui, M. S., Holehouse, A. S., Exposito-Alonso, M., Sukenik, S., Gitler, A. D. & Rhee, S.
463 Y. A prion-like protein regulator of seed germination undergoes hydration-dependent
464 phase separation. *Cell* **184,** 4284-4298.e27 (2021).
465 10. Bose, M., Lampe, M., Mahamid, J. & Ephrussi, A. Liquid-to-solid phase transition of
466 *oskar* ribonucleoprotein granules is essential for their function in *Drosophila* embryonic
467 development. *Cell* **185,** 1308-1324.e23 (2022).
468 11. Al-Husini, N., Tomares, D. T., Bitar, O., Childers, W. S. & Schrader, J. M. α-
469 Proteobacterial RNA Degradosomes Assemble Liquid-Liquid Phase-Separated RNP
470 Bodies. *Mol. Cell* **71,** 1027-1039.e14 (2018).
471 12. Pu, Y., Li, Y., Jin, X., Tian, T., Ma, Q., Zhao, Z., Lin, S., Chen, Z., Li, B., Yao, G., Leake, M.
472 C., Lo, C.-J. & Bai, F. ATP-Dependent Dynamic Protein Aggregation Regulates Bacterial
473 Dormancy Depth Critical for Antibiotic Tolerance. *Mol. Cell* **73,** 143-156.e4 (2019).
474 13. Jin, X., Lee, J.-E., Schaefer, C., Luo, X., Wollman, A. J. M., Payne-Dwyer, A. L., Tian, T.,
475 Zhang, X., Chen, X., Li, Y., McLeish, T. C. B., Leake, M. C. & Bai, F. Membraneless

organelles formed by liquid-liquid phase separation increase bacterial fitness. *Sci. Adv.* **7,** eabh2929 (2021).

14. Heinkel, F., Abraham, L., Ko, M., Chao, J., Bach, H., Hui, L. T., Li, H., Zhu, M., Ling, Y. M., Rogalski, J. C., Scurll, J., Bui, J. M., Mayor, T., Gold, M. R., Chou, K. C., Av-Gay, Y., McIntosh, L. P. & Gsponer, J. Phase separation and clustering of an ABC transporter in Mycobacterium tuberculosis. *Proc. Natl. Acad. Sci.* **116,** 16326–16331 (2019).
15. MacCready, J. S., Basalla, J. L. & Vecchiarelli, A. G. Origin and Evolution of Carboxysome Positioning Systems in Cyanobacteria. *Mol. Biol. Evol.* **37,** 1434–1451 (2020).
16. McQuail, J., Carpousis, A. J. & Wigneshweraraj, S. The association between Hfq and RNase E in long-term nitrogen-starved Escherichia coli. *Mol. Microbiol.* **117,** 54–66 (2022).
17. Azaldegui, C. A., Vecchiarelli, A. G. & Biteen, J. S. The emergence of phase separation as an organizing principle in bacteria. *Biophys. J.* **120,** 1123–1138 (2021).
18. Saurabh, S., Chong, T. N., Bayas, C., Dahlberg, P. D., Cartwright, H. N., Moerner, W. E. & Shapiro, L. ATP-responsive biomolecular condensates tune bacterial kinase signaling. *Sci. Adv.* **8,** eabm6570 (2022).
19. Lasker, K., von Diezmann, L., Zhou, X., Ahrens, D. G., Mann, T. H., Moerner, W. E. & Shapiro, L. Selective sequestration of signalling proteins in a membraneless organelle reinforces the spatial regulation of asymmetry in Caulobacter crescentus. *Nat. Microbiol.* **5,** 418–429 (2020).

497 20. Surovtsev, I. V. & Jacobs-Wagner, C. Subcellular Organization: A Critical Feature of
498 Bacterial Cell Replication. *Cell* **172,** 1271–1293 (2018).
499 21. Treuner-Lange, A. & Søgaard-Andersen, L. Regulation of cell polarity in bacteria. *J. Cell*
500 *Biol.* **206,** 7–17 (2014).
501 22. Hammarlöf, D. L., Bergman, J. M., Garmendia, E. & Hughes, D. Turnover of mRNAs is
502 one of the essential functions of RNase E. *Mol. Microbiol.* **98,** 34–45 (2015).
503 23. Ono, M. & Kuwano, M. A conditional lethal mutation in an *Escherichia coli* strain with a
504 longer chemical lifetime of messenger RNA. *J. Mol. Biol.* **129,** 343–357 (1979).
505 24. Kedersha, N., Stoecklin, G., Ayodele, M., Yacono, P., Lykke-Andersen, J., Fritzler, M. J.,
506 Scheuner, D., Kaufman, R. J., Golan, D. E. & Anderson, P. Stress granules and
507 processing bodies are dynamically linked sites of mRNP remodeling. *J. Cell Biol.* **169,**
508 871–884 (2005).
509 25. Hubstenberger, A., Courel, M., Bénard, M., Souquere, S., Ernoult-Lange, M., Chouaib,
510 R., Yi, Z., Morlot, J.-B., Munier, A., Fradet, M., Daunesse, M., Bertrand, E., Pierron, G.,
511 Mozziconacci, J., Kress, M. & Weil, D. P-Body Purification Reveals the Condensation of
512 Repressed mRNA Regulons. *Mol. Cell* **68,** 144-157.e5 (2017).
513 26. Youn, J.-Y., Dyakov, B. J. A., Zhang, J., Knight, J. D. R., Vernon, R. M., Forman-Kay, J. D. &
514 Gingras, A.-C. Properties of Stress Granule and P-Body Proteomes. *Mol. Cell* **76,** 286–
515 294 (2019).
516 27. Rathnayaka-Mudiyanselage, I., Nandana, V. & Schrader, J. Proteomic composition of
517 eukaryotic and bacterial RNA decay condensates suggests convergent evolution. *Curr.*
518 *Opin. Microbiol.* **79,** 102467 (2024).

519 28. Brengues, M., Teixeira, D. & Parker, R. Movement of Eukaryotic mRNAs Between
520 Polysomes and Cytoplasmic Processing Bodies. *Science* **310,** 486–489 (2005).
521 29. Sheth, U. & Parker, R. Decapping and Decay of Messenger RNA Occur in Cytoplasmic
522 Processing Bodies. *Science* **300,** 805–808 (2003).
523 30. Xing, W., Muhlrad, D., Parker, R. & Rosen, M. K. A quantitative inventory of yeast P body
524 proteins reveals principles of composition and specificity. *eLife* **9,** e56525 (2020).
525 31. Blake, L. A., Watkins, L., Liu, Y., Inoue, T. & Wu, B. A rapid inducible RNA decay system
526 reveals fast mRNA decay in P-bodies. *Nat. Commun.* **15,** 2720 (2024).
527 32. Wheeler, J. R., Matheny, T., Jain, S., Abrisch, R. & Parker, R. Distinct stages in stress
528 granule assembly and disassembly. *eLife* **5,** e18413 (2016).
529 33. Moon, S. L., Morisaki, T., Khong, A., Lyon, K., Parker, R. & Stasevich, T. J. Multicolour
530 single-molecule tracking of mRNA interactions with RNP granules. *Nat. Cell Biol.* **21,**
531 162–168 (2019).
532 34. Mateju, D., Franzmann, T. M., Patel, A., Kopach, A., Boczek, E. E., Maharana, S., Lee, H.
533 O., Carra, S., Hyman, A. A. & Alberti, S. An aberrant phase transition of stress granules
534 triggered by misfolded protein and prevented by chaperone function. *EMBO J.* **36,** 1669–
535 1687 (2017).
536 35. Al-Husini, N., Tomares, D. T., Pfaffenberger, Z. J., Muthunayake, N. S., Samad, M. A.,
537 Zuo, T., Bitar, O., Aretakis, J. R., Bharmal, M.-H. M., Gega, A., Biteen, J. S., Childers, W. S.
538 & Schrader, J. M. BR-Bodies Provide Selectively Permeable Condensates that Stimulate
539 mRNA Decay and Prevent Release of Decay Intermediates. *Mol. Cell* **78,** 670-682.e8
540 (2020).

541 36. Chen, H., Shiroguchi, K., Ge, H. & Xie, X. S. Genome-wide study of mRNA degradation
542 and transcript elongation in Escherichia coli. *Mol. Syst. Biol.* **11,** 781 (2015).
543 37. Barnett, T. C., Bugrysheva, J. V. & Scott, J. R. Role of mRNA Stability in Growth Phase
544 Regulation of Gene Expression in the Group A Streptococcus. *J. Bacteriol.* **189,** 1866–
545 1873 (2007).
546 38. Hambraeus, G., von Wachenfeldt, C. & Hederstedt, L. Genome-wide survey of mRNA
547 half-lives in Bacillus subtilis identifies extremely stable mRNAs. *Mol. Genet. Genomics*
548 **269,** 706–714 (2003).
549 39. Dressaire, C., Pobre, V., Laguerre, S., Girbal, L., Arraiano, C. M. & Cocaign-Bousquet, M.
550 PNPase is involved in the coordination of mRNA degradation and expression in
551 stationary phase cells of Escherichia coli. *BMC Genomics* **19,** 848 (2018).
552 40. Esquerré, T., Laguerre, S., Turlan, C., Carpousis, A. J., Girbal, L. & Cocaign-Bousquet, M.
553 Dual role of transcription and transcript stability in the regulation of gene expression in
554 Escherichia coli cells cultured on glucose at different growth rates. *Nucleic Acids Res.*
555 **42,** 2460–2472 (2014).
556 41. Morrison, J. M., Anderson, K. L., Beenken, K. E., Smeltzer, M. S. & Dunman, P. M. The
557 staphylococcal accessory regulator, SarA, is an RNA-binding protein that modulates
558 the mRNA turnover properties of late-exponential and stationary phase
559 Staphylococcus aureus cells. *Front. Cell. Infect. Microbiol.* **2,** (2012).
560 42. Zhang, M., Chang, H., Zhang, Y., Yu, J., Wu, L., Ji, W., Chen, J., Liu, B., Lu, J., Liu, Y.,
561 Zhang, J., Xu, P. & Xu, T. Rational design of true monomeric and bright photoactivatable
562 fluorescent proteins. *Nat. Methods* **9,** 727–729 (2012).

563 43. Nandana, V., Rathnayaka-Mudiyanselage, I. W., Muthunayake, N. S., Hatami, A.,
564 Mousseau, C. B., Ortiz-Rodríguez, L. A., Vaishnav, J., Collins, M., Gega, A.,
565 Mallikaarachchi, K. S., Yassine, H., Ghosh, A., Biteen, J. S., Zhu, Y., Champion, M. M.,
566 Childers, W. S. & Schrader, J. M. The BR-body proteome contains a complex network of
567 protein-protein and protein-RNA interactions. *Cell Rep.* **42,** (2023).
568 44. Hardwick, S. W., Chan, V. S. Y., Broadhurst, R. W. & Luisi, B. F. An RNA degradosome
569 assembly in Caulobacter crescentus. *Nucleic Acids Res.* **39,** 1449–1459 (2011).
570 45. Ester, M., Kriegel, H.-P., Sander, J. & Xu, X. A density-based algorithm for discovering
571 clusters in large spatial databases with noise. in *Proc. Second Int. Conf. Knowl. Discov.*
572 *Data Min*. 226–231 (AAAI Press, 1996).
573 46. Kroschwald, S., Maharana, S., Mateju, D., Malinovska, L., Nüske, E., Poser, I., Richter, D.
574 & Alberti, S. Promiscuous interactions and protein disaggregases determine the
575 material state of stress-inducible RNP granules. *eLife* **4,** e06807 (2015).
576 47. Kroschwald, S., Maharana, S. & Simon, A. Hexanediol: a chemical probe to investigate
577 the material properties of membrane-less compartments. *Matters* (2017).
578 doi:10.19185/matters.201702000010
579 48. Lin, Y., Mori, E., Kato, M., Xiang, S., Wu, L., Kwon, I. & McKnight, S. L. Toxic PR Poly-
580 Dipeptides Encoded by the C9orf72 Repeat Expansion Target LC Domain Polymers. *Cell*
581 **167,** 789-802.e12 (2016).
582 49. Hondele, M., Sachdev, R., Heinrich, S., Wang, J., Vallotton, P., Fontoura, B. M. A. & Weis,
583 K. DEAD-box ATPases are global regulators of phase-separated organelles. *Nature* **573,**
584 144–148 (2019).

585 50. Deng, Y., Beahm, D. R., Ionov, S. & Sarpeshkar, R. Measuring and modeling energy and
586 power consumption in living microbial cells with a synthetic ATP reporter. *BMC Biol.* **19,**
587 101 (2021).
588 51. Parry, B. R., Surovtsev, I. V., Cabeen, M. T., O'Hern, C. S., Dufresne, E. R. & Jacobs-
589 Wagner, C. The Bacterial Cytoplasm Has Glass-like Properties and Is Fluidized by
590 Metabolic Activity. *Cell* **156,** 183–194 (2014).
591 52. Weber, S. C., Spakowitz, A. J. & Theriot, J. A. Nonthermal ATP-dependent fluctuations
592 contribute to the in vivo motion of chromosomal loci. *Proc. Natl. Acad. Sci.* **109,** 7338–
593 7343 (2012).
594 53. Russell, R., Jarmoskaite, I. & Lambowitz, A. M. Toward a molecular understanding of
595 RNA remodeling by DEAD-box proteins. *RNA Biol.* **10,** 44–55 (2013).
596 54. Li, X.-Z., Plésiat, P. & Nikaido, H. The Challenge of Efflux-Mediated Antibiotic Resistance
597 in Gram-Negative Bacteria. *Clin. Microbiol. Rev.* **28,** 337–418 (2015).
598 55. Nathans, D. Puromycin inhibition of protein synthesis: incorporation of puromycin into
599 peptide chains. *Proc. Natl. Acad. Sci.* **51,** 585–592 (1964).
600 56. Oh, E., Becker, A. H., Sandikci, A., Huber, D., Chaba, R., Gloge, F., Nichols, R. J., Typas,
601 A., Gross, C. A., Kramer, G., Weissman, J. S. & Bukau, B. Selective Ribosome Profiling
602 Reveals the Cotranslational Chaperone Action of Trigger Factor In Vivo. *Cell* **147,** 1295–
603 1308 (2011).
604 57. Pontes, M. H., Sevostyanova, A. & Groisman, E. A. When Too Much ATP Is Bad for
605 Protein Synthesis. *J. Mol. Biol.* **427,** 2586–2594 (2015).

606 58. Stouthamer, A. H. A theoretical study on the amount of ATP required for synthesis of
607 microbial cell material. *Antonie Van Leeuwenhoek* **39,** 545–565 (1973).
608 59. Patel, A., Lee, H. O., Jawerth, L., Maharana, S., Jahnel, M., Hein, M. Y., Stoynov, S.,
609 Mahamid, J., Saha, S., Franzmann, T. M., Pozniakovski, A., Poser, I., Maghelli, N., Royer,
610 L. A., Weigert, M., Myers, E. W., Grill, S., Drechsel, D., Hyman, A. A. & Alberti, S. A
611 Liquid-to-Solid Phase Transition of the ALS Protein FUS Accelerated by Disease
612 Mutation. *Cell* **162,** 1066–1077 (2015).
613 60. Molliex, A., Temirov, J., Lee, J., Coughlin, M., Kanagaraj, A. P., Kim, H. J., Mittag, T. &
614 Taylor, J. P. Phase Separation by Low Complexity Domains Promotes Stress Granule
615 Assembly and Drives Pathological Fibrillization. *Cell* **163,** 123–133 (2015).
616 61. Zhang, H., Elbaum-Garfinkle, S., Langdon, E. M., Taylor, N., Occhipinti, P., Bridges, A. A.,
617 Brangwynne, C. P. & Gladfelter, A. S. RNA Controls PolyQ Protein Phase Transitions.
618 *Mol. Cell* **60,** 220–230 (2015).
619 62. Lin, Y., Protter, D. S. W., Rosen, M. K. & Parker, R. Formation and Maturation of Phase-
620 Separated Liquid Droplets by RNA-Binding Proteins. *Mol. Cell* **60,** 208–219 (2015).
621 63. Xiang, S., Kato, M., Wu, L. C., Lin, Y., Ding, M., Zhang, Y., Yu, Y. & McKnight, S. L. The LC
622 Domain of hnRNPA2 Adopts Similar Conformations in Hydrogel Polymers, Liquid-like
623 Droplets, and Nuclei. *Cell* **163,** 829–839 (2015).
624 64. Watanabe, H. Viscoelasticity and dynamics of entangled polymers. *Prog. Polym. Sci.*
625 **24,** 1253–1403 (1999).
626 65. Halfmann, R. A glass menagerie of low complexity sequences. *Curr. Opin. Struct. Biol.*
627 **38,** 18–25 (2016).

628 66. Mittag, T. & Pappu, R. V. A conceptual framework for understanding phase separation
629 and addressing open questions and challenges. *Mol. Cell* **82,** 2201–2214 (2022).
630 67. Boke, E., Ruer, M., Wühr, M., Coughlin, M., Lemaitre, R., Gygi, S. P., Alberti, S., Drechsel,
631 D., Hyman, A. A. & Mitchison, T. J. Amyloid-like Self-Assembly of a Cellular
632 Compartment. *Cell* **166,** 637–650 (2016).
633 68. Linsenmeier, M., Hondele, M., Grigolato, F., Secchi, E., Weis, K. & Arosio, P. Dynamic
634 arrest and aging of biomolecular condensates are modulated by low-complexity
635 domains, RNA and biochemical activity. *Nat. Commun.* **13,** 3030 (2022).
636 69. Bertrand, E., Chartrand, P., Schaefer, M., Shenoy, S. M., Singer, R. H. & Long, R. M.
637 Localization of ASH1 mRNA Particles in Living Yeast. *Mol. Cell* **2,** 437–445 (1998).
638 70. Tutucci, E., Vera, M., Biswas, J., Garcia, J., Parker, R. & Singer, R. H. An improved MS2
639 system for accurate reporting of the mRNA life cycle. *Nat. Methods* **15,** 81–89 (2018).
640 71. Nandana, V., Al-Husini, N., Vaishnav, A., Dilrangi, K. H. & Schrader, J. M. Caulobacter
641 crescentus RNase E condensation contributes to autoregulation and fitness. *Mol. Biol.*
642 *Cell* **35,** ar104 (2024).
643 72. Awram, P. & Smit, J. The Caulobacter crescentus Paracrystalline S-Layer Protein Is
644 Secreted by an ABC Transporter (Type I) Secretion Apparatus. *J. Bacteriol.* **180,** 3062–
645 3069 (1998).
646 73. Wheeler, R. T. & Shapiro, L. Differential Localization of Two Histidine Kinases
647 Controlling Bacterial Cell Differentiation. *Mol. Cell* **4,** 683–694 (1999).

648 74. Radhakrishnan, S. K., Thanbichler, M. & Viollier, P. H. The dynamic interplay between a
649 cell fate determinant and a lysozyme homolog drives the asymmetric division cycle of
650 Caulobacter crescentus. *Genes Dev.* **22,** 212–225
651 75. Ryan, K. R., Judd, E. M. & Shapiro, L. The CtrA Response Regulator Essential for
652 *Caulobacter crescentus* Cell-cycle Progression Requires a Bipartite Degradation Signal
653 for Temporally Controlled Proteolysis. *J. Mol. Biol.* **324,** 443–455 (2002).
654 76. Wortinger, M., Sackett, M. J. & Brun, Y. V. CtrA mediates a DNA replication checkpoint
655 that prevents cell division in Caulobacter crescentus. *EMBO J.* **19,** 4503–4512 (2000).
656 77. Laub, M. T., Chen, S. L., Shapiro, L. & McAdams, H. H. Genes directly controlled by
657 CtrA, a master regulator of the Caulobacter cell cycle. *Proc. Natl. Acad. Sci.* **99,** 4632–
658 4637 (2002).
659 78. Laub, M. T., McAdams, H. H., Feldblyum, T., Fraser, C. M. & Shapiro, L. Global Analysis
660 of the Genetic Network Controlling a Bacterial Cell Cycle. *Science* **290,** 2144–2148
661 (2000).
662 79. Quon, K. C., Marczynski, G. T. & Shapiro, L. Cell Cycle Control by an Essential Bacterial
663 Two-Component Signal Transduction Protein. *Cell* **84,** 83–93 (1996).
664 80. LeCuyer, K. A., Behlen, L. S. & Uhlenbeck, O. C. Mutants of the Bacteriophage MS2 Coat
665 Protein That Alter Its Cooperative Binding to RNA. *Biochemistry* **34,** 10600–10606
666 (1995).
667 81. Garcia, J. F. & Parker, R. MS2 coat proteins bound to yeast mRNAs block 5' to 3'
668 degradation and trap mRNA decay products: implications for the localization of mRNAs
669 by MS2-MCP system. *RNA* **21,** 1393–1395 (2015).

670 82. Heinrich, S., Sidler, C. L., Azzalin, C. M. & Weis, K. Stem–loop RNA labeling can affect
671 nuclear and cytoplasmic mRNA processing. *RNA* **23,** 134–141 (2017).
672 83. Garcia, J. F. & Parker, R. Ubiquitous accumulation of 3' mRNA decay fragments in
673 Saccharomyces cerevisiae mRNAs with chromosomally integrated MS2 arrays. *RNA* **22,**
674 657 (2016).
675 84. Guan, J., Hurto, R. L., Rai, A., Azaldegui, C. A., Ortiz-Rodríguez, L. A., Biteen, J. S.,
676 Freddolino, L. & Jakob, U. HP-Bodies – Ancestral Condensates that Regulate RNA
677 Turnover and Protein Translation in Bacteria. 2025.02.06.636932 Preprint at
678 https://doi.org/10.1101/2025.02.06.636932 (2025)
679 85. Goldberger, O., Szoke, T., Nussbaum-Shochat, A. & Amster-Choder, O. Heterotypic
680 phase separation of Hfq is linked to its roles as an RNA chaperone. *Cell Rep.* **41,**
681 111881 (2022).
682 86. Pei, L., Xian, Y., Yan, X., Schaefer, C., Syeda, A. H., Howard, J., Liao, H., Bai, F., Leake, M.
683 C. & Pu, Y. Bacterial stress granule protects mRNA through ribonucleases exclusion.
684 2024.04.27.591437 Preprint at https://doi.org/10.1101/2024.04.27.591437 (2024)
685 87. Bollen, C., Louwagie, S., Deroover, F., Duverger, W., Khodaparast, L., Khodaparast, L.,
686 Hofkens, D., Schymkowitz, J., Rousseau, F., Dewachter, L. & Michiels, J. Composition
687 and liquid-to-solid maturation of protein aggregates contribute to bacterial dormancy
688 development and recovery. *Nat. Commun.* **16,** 1046 (2025).
689 88. Mudd, E. A., Krisch, H. M. & Higgins, C. F. RNase E, an endoribonuclease, has a general
690 role in the chemical decay of Escherichia coli mRNA: evidence that rne and ams are the
691 same genetic locus. *Mol. Microbiol.* **4,** 2127–2135 (1990).

692 89. Górna, M. W., Carpousis, A. J. & Luisi, B. F. From conformational chaos to robust
693 regulation: the structure and function of the multi-enzyme RNA degradosome. *Q. Rev.*
694 *Biophys*. **45,** 105–145 (2012).
695 90. Bandyra, K. J., Bouvier, M., Carpousis, A. J. & Luisi, B. F. The social fabric of the RNA
696 degradosome. *Biochim. Biophys. Acta BBA - Gene Regul. Mech.* **1829,** 514–522 (2013).
697 91. Schramm, F. D., Schroeder, K., Alvelid, J., Testa, I. & Jonas, K. Growth-driven
698 displacement of protein aggregates along the cell length ensures partitioning to both
699 daughter cells in Caulobacter crescentus. *Mol. Microbiol.* **111,** 1430–1448 (2019).
700 92. Wortinger, M. A., Quardokus, E. M. & Brun, Y. V. Morphological adaptation and inhibition
701 of cell division during stationary phase in Caulobacter crescentus. *Mol. Microbiol.* **29,**
702 963–973 (1998).
703 93. Lee, K., Zhan, X., Gao, J., Qiu, J., Feng, Y., Meganathan, R., Cohen, S. N. & Georgiou, G.
704 RraA: a Protein Inhibitor of RNase E Activity that Globally Modulates RNA Abundance in
705 E. coli. *Cell* **114,** 623–634 (2003).
706 94. Górna, M. W., Pietras, Z., Tsai, Y.-C., Callaghan, A. J., Hernández, H., Robinson, C. V. &
707 Luisi, B. F. The regulatory protein RraA modulates RNA-binding and helicase activities of
708 the E. coli RNA degradosome. *RNA* **16,** 553–562 (2010).